INTERNATIONAL JOURNAL FOR NUMERICAL METHODS IN ENGINEERING
Int. J. Numer. Meth. Engng (2010)
View this article online at wileyonlinelibrary.com. DOI: 10.1002/nme.2995

Multi-scale modeling of surface effect via the boundary Cauchy–Born method

M. J. Abdolhosseini Qomi[‡], A. Aghaei[§] and A. R. Khoei[*, †, ¶]

Center of Excellence in Structures and Earthquake Engineering, Department of Civil Engineering, Sharif University of Technology, P.O. Box 11365-9313, Tehran, Iran

SUMMARY

In this paper, a novel multi-scale approach is developed for modeling of the surface effect in crystalline nano-structures. The technique is based on the Cauchy–Born hypothesis in which the strain energy density of the equivalent continua is calculated by means of inter-atomic potentials. The notion of introducing the surface effect in the finite element method is based on the intrinsic function of quadratures, called as an indicator of material behavior. The information of quadratures is derived by interpolating the data from probable representative atoms in their proximity. The technique is implemented by the definition of reference boundary CB elements, which enable to capture not only the surface but also the edge and corner effects. As the surface effect is important in small-scale simulation, the relative number of boundary CB elements increases which leads to predomination of boundary effects in the model. In order to implement the equivalent continua in boundary value problems, the updated-Lagrangian formulation of nonlinear finite element is derived. The numerical simulation of the proposed model together with the direct comparison with fully atomistic model indicates that the technique provides promising results for facile modeling of boundary effects and investigating its effect on the mechanical response of metallic nano-scale devices. Copyright © 2010 John Wiley & Sons, Ltd.

Received 4 January 2009; Revised 16 September 2009; Accepted 15 June 2010

KEY WORDS: boundary Cauchy–Born; surface effect; multi-scale modeling; molecular dynamics

1. INTRODUCTION

Mindboggling advances in the nanotechnology have altered the countenance of science and technology. The promising results of this fledgling branch of science have absorbed a commensurate

*Correspondence to: A. R. Khoei, Center of Excellence in Structures and Earthquake Engineering, Department of Civil Engineering, Sharif University of Technology, P.O. Box 11365-9313, Tehran, Iran.
†E-mail: arkhoei@sharif.edu
‡Current address: Department of Civil and Environmental Engineering, Massachusetts Institute of Technology, 77 Massachusetts Avenue, 02139 Cambridge, MA, U.S.A.
§Current address: Department of Civil and Environmental Engineering, Carnegie Mellon University, 15213-3890, Pittsburgh, PA, U.S.A.
¶Professor.

portion of the research community. The experimental efforts have led to the synthesis of two distinct classes of nano-materials; the nano-structured materials in which the characteristic length of their ingredient micro-structures is in the scale of nanometer, and the nano-sized structural elements in which at least one of the overall dimensions is in the range of nanometer. Despite the fact that the structural elements are in macro-scale, the nano-scale materials are strongly influenced by the surface effects.

The basis of surface effect is mainly due to the nature of chemical bonding at the surface of structures, which is absolutely different from the interior atoms. Sander [1] demonstrated that the reduced atomic coordination of atoms near the surface induces the redistribution of electronic charge, which alters the binding of atoms. The loss of neighbors reduces the electron density of atoms in the proximity of surface. The disparity of electron density between the surface and bulk atoms provokes the decrease of inter-atomic distance and the increase of electron density of external atoms. It can be therefore deduced that the interior part of structure is exerting stress on the exterior boundaries [2]. It was reported in the early works of Gibbs [3] that the surface stress in solids, as a thermodynamic parameter, differs from the surface energy. The available models that incorporate the surface effect can be classified into two categories; the analytical method and numerical approaches. The continuum theory of surface stress, known as augmented continuum theory, was proposed by Gurtin and Murdoch [4, 5]. It is worth mentioning that the brilliant notion embedded in the prolific work of Gurtin has been pursued by other researchers as a common guideline due to its simplified form. Miller and Shenoy [6] and Shenoy [7] proposed the augmented continuum theory to demonstrate the size dependency of material properties at nano-scale. Lim and He [8] and He *et al.* [9] derived a model based on the abovementioned idea, which is able to capture the nonlinear size-dependent response of thin elastic films with nano-dimensional thickness. Sharma *et al.* [10] used the augmented continuum method for the investigation of size-dependent nano-inhomogeneities. However, the presence of coupled surface stresses and the nonstandard boundary conditions in the general formulation of augmented continuum hinder the prevalent use of this method. In addition, the extra atomistic simulations are required for the calculation of surface elastic constants. Nevertheless, Wei *et al.* [11] applied the Gurtin's theory in finite element approach to study the behavior of nano-systems. The other noteworthy approach was presented by Dingreville *et al.* [12] based on the surface free energy to derive the general formulation for the elastic behavior of nano-wires and nano-plates.

Park *et al.* [13] proposed the surface Cauchy–Born model, in which the potential energy of the system is decomposed into the bulk and surface components. They computed the potential energy in both parts of the domain using the Cauchy–Born hypothesis and the surface constants derived by numerical simulations. Based on this idea, they developed a nonlinear finite element model to simulate different nano-structures, such as metallic nano-wires [14] and silicon nano-structures [15]. However, the surface Cauchy–Born model of Park has two weaknesses. First, the method only presents the effect of surface and cannot capture the effects of edge and corner, which have significant influences in the stress distribution over the body. Second, the finite element formulation of this method is decomposed into two different parts, in which its implementation requires some additional terms.

As a practical guideline, it is suggested to use the reference boundary elements in the boundary of concurrent multi-scale methods, such as quasi-continuum [16, 17], the bridging scale method [18] and the bridging domain method [19]. The lack of proper method to incorporate the surface effect is explicitly expressed in quasi-continuum modeling of silicon nano-structures at finite temperature [20]. In the present paper, a novel approach is presented to model the surface effect

DOI: 10.1002/nme

by means of the Cauchy–Born hypothesis. The intrinsic notion of this method is embedded in the function of quadratures, denoted by the integration points in the finite element method. In fact, each quadrature point of model represents the atomistic medium, which can be interpreted in a way that the information at each specific quadrature can be derived by averaging the information from nearby representative atoms. In order to appropriately implement the model, the approach is used together with the reference boundary element, which enables to capture the stress over the body from the surface of structure to the edges and corners. The reference boundary elements are astonishingly easy to apply in the surface effect simulation of curved surfaces.

This paper is organized into the following sections. In Section 2, the concept of Cauchy–Born hypothesis is demonstrated. In Section 3, the constitutive laws governing the equivalent continuum are derived based on the Cauchy–Born hypothesis. In order to model the real metallic behavior in nano-structures, the Sutton–Chen many-body potential is proposed for the calculation of stress and elasticity tensors. In Section 4, the updated-Lagrangian formulation of the equivalent continua is presented. In Section 5, the concept of boundary Cauchy–Born method is comprehensively discussed and the reference surface, edge and corner elements are defined. In this section, the computational algorithm is presented for the numerical implementation of the model. In order to verify the validity of the proposed model, the results of two models are directly compared with the fully atomistic models in Section 6. Finally, some concluding remarks are provided in Section 7.

2. CAUCHY–BORN HYPOTHESIS

The Cauchy–Born (CB) hypothesis is a homogenization assumption in the molecular theory of elasticity, in which the atomic positions are related to the continuum field through the deformation gradient F [21]. In THE classical continuum mechanics, the deformation gradient is a second-order tensor that maps an infinitesimal vector dX in the material configuration to its counterpart dx in the spatial configuration as [22]

$$\mathrm{d}x_i = F_{ij}\,\mathrm{d}X_j \tag{1}$$

where F_{ij} is the partial derivative $\mathrm{L}x_i/\mathrm{L}X_j$ in Cartesian coordinate. The well-known CB hypothesis assumes that if the boundaries of a defect-free and single-crystalline infinite lattice are subjected to a homogeneous deformation, the entire lattice deforms according to the abovementioned deformation gradient [23]. Hence, if A denotes a lattice vector in the material configuration and a indicates the same vector in the spatial configuration, the CB hypothesis demonstrates that the relationship between these two vectors can be established by (Figure 1)

$$\mathrm{a} = \mathrm{F}.\mathrm{A} \tag{2}$$

From the mathematical point of view, an approximation error entails in the above equation since the lattice vectors have finite lengths. However, it can be applicable as long as the lattice deformation is homogeneous in the scale of lattice vectors. In fact, the CB hypothesis must be employed wherever a description of underlying atomic structure is valid. This issue has been recently investigated by Khoei *et al.* [24] and Aghaei *et al.* [25] to derive a validity surface for the CB hypothesis. They produced a criterion for the validity of CB hypothesis by comparatively investigating the atomistic and continuous models, in which the crystalline lattice deforms homogeneously.

DOI: 10.1002/nme

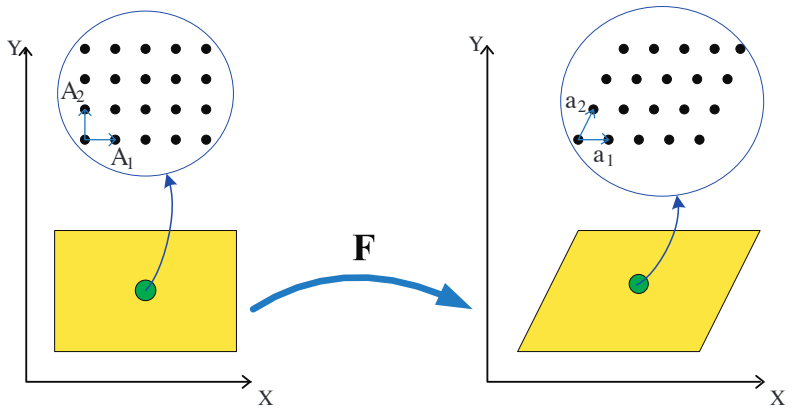

Figure 1. Schematic description of CB hypothesis: the lattice vectors are deformed by means of the deformation gradient F.

3. A CONTINUUM-BASED CAUCHY–BORN HYPOTHESIS

In isothermal elastic processes, the hyperelastic theory can be used to model the homogeneous deformation of crystalline structure since the rate of recoverable strain energy is identical to the rate of work done on the structure. In hyperelasticity, the first Piola–Kirchhoff stress tensor (1PK) P can be derived by [26]

$$P_{ij} = \frac{\partial w_o}{\partial F_{ji}} \tag{3}$$

where w_0 is the strain energy function per unit undeformed volume. In the behavior of crystalline structures via the continuum mechanics, the strain energy density must be calculated using the inter-atomic potentials. Despite simplicity and rational computational expense of pair-wise potentials, such as the Lennard–Jones potential, they are incapable of modeling the behavior of metallic crystalline structures. For instance, in spite of the convexity of their outer surface, these potentials depict concave surfaces for metallic nano-structures. Moreover, the pair-wise potentials cannot correctly illustrate the Cauchy relation in the elasticity of metallic structures, i.e. $C_{12} \neq C_{44}$ [27]. Therefore, the Sutton–Chen many-body potential is used here to calculate the strain energy density. This potential has been developed to produce an applicable potential, which is efficient for numerical simulation of atomistic medium. The Sutton–Chen potential is defined by [28, 29]

$$\begin{aligned} E_p^{\mathrm{SC}} &= \varepsilon \left[\frac{1}{2} \sum_{q \neq p} U_{pq}(r_{pq}) - C \sqrt{\rho_p} \right] \\ U_{pq}(r_{pq}) &= \left(\frac{a}{r_{pq}} \right)^n, \quad \rho_p = \sum_{q \neq p} \left(\frac{a}{r_{pq}} \right)^m \end{aligned} \tag{4}$$

where E_p^{SC} is the potential energy of pth atomic site due to the embedding energy function ρ_i and the repulsive pair-wise interaction U_{pq}. The term r_{pq} is the inter-atomic distance between the

DOI: 10.1002/nme

host atom p and its neighboring atom q in the deformed configuration. In the above formulation, a is the lattice parameter and ε, m, n and C are the constants, which can be obtained by fitting the experimental data [28]. Thus, the strain energy density at the atomic site p is calculated by means of

$$w_0^p = \frac{\varepsilon}{\Omega_0^p}\left[\frac{1}{2}\sum_{q\neq p} U_{pq}(r_{pq}) - C\sqrt{q_p}\right] \tag{5}$$

where Ω_0^p is the local atomic volume dedicated to the pth atomic position and is generally calculated by the Voronoi polyhedron algorithm. For FCC materials, the local atomic volume is equal to $a^3/4$. According to the CB hypothesis, if the inter-atomic vector is considered as the lattice vector, it can be assumed that it deforms with respect to the deformation gradient imposed on this vector. As a result, the strain energy density can be assumed as a function of deformation gradient. In addition, the stress at all atomic positions is identical since all atoms experience similar deformation gradient in the bulk of material. Hence, the index that indicates the atomic position can be omitted implicitly. Using Equations (3) and (5), the first PK stress tensor can be derived as

$$P_{ij} = \frac{\varepsilon}{2\Omega_0}\sum_{q\neq p}\left[\frac{\partial V(r_{pq})}{\partial r_{pq}} - \frac{c}{\sqrt{q_p}}\frac{\partial q_p}{\partial r_{pq}}\right]\frac{\partial r_{pq}}{\partial F_{ji}} \tag{6}$$

where the host atom is indicated by index p and its neighbors are shown by index q. The term $\partial r_{pq}/\partial F_{ji}$ can be calculated by

$$\frac{\partial r_{pq}}{\partial F_{iJ}} = \frac{r_{pq}^j r_{pq}^J}{r_{pq}} F_{iJ}^{-1} \tag{7}$$

where r_{pq}^j denotes the distance between the host atom p and its neighbor q in the jth direction. The first PK stress, as a Lagrangian measure is not a symmetric tensor and as a result, it is not suitable for the implementation in the computational algorithm. Thus, it must be converted to other stress measures. The Cauchy stress, as an Eulerian measure, can be calculated simply using Equation (8) as

$$\sigma_{ij} = \frac{1}{J} F_{ik} P_{kj} \tag{8}$$

where J is the determinant of deformation gradient tensor, known as Jacobian.

The first elasticity tensor $C^{(1)}$ is a fourth-order tensor that relates the rate of deformation gradient to its stress conjugate. The rate of first PK stress can be written as

$$\dot{P}_{ij} = C_{ijkl}^{(1)} \dot{F}_{kl} \tag{9}$$

The above relation is expressed in terms of rates since Equation (6) has explicitly a nonlinear entity. In the hyperelasticy model, the first elasticity tensor is the second derivative of strain energy density with respect to the deformation gradient

$$C_{ijkl}^{(1)} = \frac{\partial^2 w_0}{\partial F_{ji}\partial F_{lk}} \tag{10}$$

DOI: 10.1002/nme

Considering the CB hypothesis and calculating the strain energy density from Equation (5), the first elasticity tensor can be derived as

$$C_{ijkl}^{(1)} = \frac{\varepsilon}{2\chi_0}\left(\sum_{q\neq p}\left[\frac{\partial^2 V(r_{pq})}{\partial r_{pq}^2}\frac{\partial r_{pq}}{\partial F_{LK}} - \frac{c}{\sqrt{q_p}}\frac{\partial^2 q_p}{\partial r_{pq}^2}\frac{\partial r_{pq}}{\partial F_{LK}}\right]\frac{\partial r_{pq}}{\partial F_{ji}}\right.$$
$$+\frac{c}{2q_p\sqrt{q_p}}\left(\sum_{q\neq p}\frac{\partial q_p}{\partial r_{pq}}\frac{\partial r_{pq}}{\partial F_{ji}}\right)\left(\sum_{m\neq p}\frac{\partial q_p}{\partial r_{pm}}\frac{\partial r_{pm}}{\partial F_{lk}}\right)$$
$$\left.+\sum_{q\neq p}\left[\frac{\partial V(r_{pq})}{\partial r_{pq}} - \frac{c}{\sqrt{q_p}}\frac{\partial q_p}{\partial r_{pq}}\right]\frac{\partial^2 r_{pq}}{\partial F_{ji}\partial F_{lk}}\right) \tag{11}$$

where the term $\partial^2 r_{pq}/\partial F_{ji}\partial F_{lk}$ can be calculated via the following relation:

$$\frac{\partial^2 r_{pq}}{\partial F_{ji}\partial F_{lk}} = \frac{(r_{pq}^2\delta_{jl} - r_{pq}^j r_{pq}^l)r_{pq}^I r_{pq}^K}{r_{pq}^3}F_{kK}^{-1}F_{iI}^{-1} \tag{12}$$

where δ is the Kronecker delta in indicial notation. Similar to the first PK stress, the first elasticity tensor is a Lagrangian measure which is not symmetric. In the updated Lagrangian formulation of the finite element method, another version of elasticity tensor is pervasively used which is known as Truesdell elasticity tensor $C^{\tau T}$. This fourth-order tensor can be derived from the first elasticity tensor through the following relation:

$$C_{ijkl}^{\tau T} = \frac{1}{J}F_{im}F_{ln}C_{mjnk}^{(1)} - \delta_{jk}\tau_{il} \tag{13}$$

The continua defined through Equations (6)–(11) represents a nonlinear medium, which can be considered as an equivalent for a metallic lattice structure. In order to employ this continuum in the boundary value problems together with the arbitrary form of boundaries and constraints, the constitutive equations are presented using the nonlinear finite element method.

4. NONLINEAR FINITE ELEMENT ANALYSIS OF EQUIVALENT CONTINUA

The nonlinearities in FEM arise from two main sources; the constitutive and geometric nonlinearities, in which the latter is mainly due to large deformations [30]. In this work, the only source of nonlinearity is due to constitutive laws governing the overall behavior of equivalent medium. Whether the displacement is small or large, the equilibrium equation between the internal and external forces is absolutely mandatory. In general, the equilibrium criterion of a body in spatial coordinate can be written as

$$\frac{\partial \tau_{ji}}{\partial x_j} + \rho b_i = \rho \ddot{u}_i \tag{14}$$

where ρ is the density of material in deformed configuration and b_i is the body force in the ith direction. According to the virtual work theorem, the above formulation can be converted to its weak form by multiplying Equation (14) to a virtual velocity field $\delta\dot{u}_i$, and integrating over the

DOI: 10.1002/nme

entire body. It is worth mentioning that this nonzero virtual field must be small and consistent with the boundary conditions. Thus,

$$\int_{\Omega} \left(\frac{\partial \sigma_{ji}}{\partial x_j} + \rho b_i - \rho \ddot{u}_i \right) \delta u_i \, d\Omega = 0 \tag{15}$$

Manipulating the above equation and using the divergence theorem, Equation (15) can be transformed into

$$\int_{\Omega} \frac{\partial (\delta u_i)}{\partial x_j} \sigma_{ji} \, d\Omega - \int_{\Omega} \delta u_i \rho b_i \, d\Omega - \int_{\Gamma} \delta u_i t_i \, d\Gamma + \int_{\Omega} \delta u_i \rho \ddot{u}_i \, d\Omega \tag{16}$$

where t_i is the traction vector applied on the boundary of body in the ith direction. In order to develop a finite element formulation, Equation (16) is numerically solved for a spatial discrete domain. As the standard procedure of finite element method, the initial domain Ω is divided into elements Ω^e such that $\Omega = \cup_e \Omega^e$. Traditionally, the displacement within an element can be derived based on the nodal displacements. Therefore, if the coordinate of nodal point I at time t of spatial configuration is denoted by matrix $x_I(t)$, the coordinate of an arbitrary point $x_i(X, t)$ can be derived by means of shape functions $N_I(X)$ as

$$x_i(X, t) = N_I(X) x_{iI}(t) \tag{17}$$

where indices I and i indicate the node number and general directions, respectively. In the above equation, X denotes the nodal coordinate in the undeformed configuration. Moreover, the shape functions can be used to derive the displacement, velocity and acceleration at any arbitrary point of domain. The discretization process is routinely applicable to the virtual velocities of Equation (16). Hence,

$$\frac{\partial (\delta u_i)}{\partial x_j} = \frac{\partial (\delta v_i)}{\partial x_j} = \delta L_{ij} = \frac{\partial N_I(X)}{\partial x_j} \delta u_{iI}(t) \tag{18}$$

where L is the velocity gradient tensor in the continuum mechanics. As can be seen from Equation (18), the virtual velocity field $\delta u_{iI}(t)$ can be derived by some manipulation. Considering Equations (16) and (18), the term δu_{iI} can be omitted from the integrals of Equation (16). Thus, Equation (16) can be rewritten as

$$\int_{\Omega} \frac{\partial N_I}{\partial x_j} \sigma_{ji} \, d\Omega - \int_{\Omega} N_I \rho b_i \, d\Omega - \int_{\Gamma} N_I t_i \, d\Gamma + \int_{\Omega} N_I \rho \ddot{u}_i \, d\Omega = 0 \tag{19}$$

In the above equation, the first integral indicates the internal forces $\mathrm{f}^{\mathrm{int}}$, and the sum of second and third terms represent the external forces $\mathrm{f}^{\mathrm{ext}}$, implemented on the nodal points. The last integral demonstrates the inertial forces due to the acceleration of system. In the simulation of quasi-static processes, the fourth term is negligible and can be eliminated from the final formulation. As the nonlinear finite element equation presented in Equation (19) must be solved by an iterative approach, a residual force function w is defined as

$$\mathrm{w} = \mathrm{f}^{\mathrm{int}} - \mathrm{f}^{\mathrm{ext}} = 0 \tag{20}$$

DOI: 10.1002/nme

In nonlinear problems, Equation (20) must be solved by an incremental manner due to intrinsic nonlinear nature of the governing equations. Thus,

$$\dot{\mathsf{w}} = \dot{\mathsf{f}}^{\text{int}} - \dot{\mathsf{f}}^{\text{ext}} = 0 \tag{21}$$

In order to obtain the displacement field, Equation (21) is solved numerically to satisfy the balance between the internal and external nodal forces. Thus, Equation (21) can be rewritten as

$$\mathsf{w} = \mathrm{K}\,\mathrm{v} - \dot{\mathsf{f}}^{\text{ext}} = 0 \tag{22}$$

where K is the total stiffness matrix of system. In order to derive the updated Lagrangian form of nonlinear finite element method, the first term of Equation (19) is rewritten in terms of objective Eulerian measures. Manipulating the internal forces $\dot{\mathsf{f}}^{\text{int}}$ by the means of basic continuum mechanics relations, the Eulerian description can be written as

$$\dot{f}_{Ii}^{\text{int}} = \int_{\mathsf{X}^0} \frac{\mathrm{L}N_I}{\mathrm{L}x_k} (\mathsf{s}_{ki}^{\nabla c} + \mathsf{s}_{kl} L_{il})\, \mathrm{d}\mathsf{X}^0 \tag{23}$$

where $\dot{f}_{Ii}^{\text{int}}$ is the incremental internal force at the Ith node and ith direction, s is the Kirchhoff stress and $\mathsf{s}^{\nabla c}$ denotes the objective rate of Kirchhoff stress. It must be noted that the integration over X^0 must be taken in the undeformed configuration. In order to convert this integration into the integration over spatial configuration, a Jacobian is imposed on Equation (23) as [31]

$$\dot{f}_{Ii}^{\text{int}} = \int_{\mathsf{X}} \frac{\mathrm{L}N_I}{\mathrm{L}x_k} (\mathsf{r}_{ki}^{\nabla c} + \mathsf{s}_{kl} L_{il})\, \mathrm{d}\mathsf{X} \tag{24}$$

where $\mathsf{r}^{\nabla c}$ is the objective rate of Cauchy stress tensor. Equation (24) mainly consisted of two distinct parts; the incremental material internal force $\dot{\mathsf{f}}^{\text{mat}}$, and the incremental geometric internal force $\dot{\mathsf{f}}^{\text{geo}}$ defined as

$$\dot{f}_{Ii}^{\text{mat}} = \int_{\mathsf{X}} \frac{\mathrm{L}N_I}{\mathrm{L}x_k} \mathsf{r}_{ki}^{\nabla T}\, \mathrm{d}\mathsf{X} \tag{25}$$

$$\dot{f}_{Ii}^{\text{geo}} = \int_{\mathsf{X}} \frac{\mathrm{L}N_I}{\mathrm{L}x_k} \mathsf{r}_{kl} L_{il}\, \mathrm{d}\mathsf{X} \tag{26}$$

In Equation (25), the objective rate of Cauchy stress can be expressed in terms of its conjugate strain measure, i.e. the rate of deformation tensor D and Truesdell elasticity tensor

$$\mathsf{r}_{ij}^{\nabla T} = C_{ijkl}^{\mathsf{r}\,T} D_{kl} \tag{27}$$

Inserting Equation (27) into Equation (25) and manipulating the notation D_{kl} as the symmetric part of velocity gradient tensor, and considering the symmetry of Truesdell elasticity tensor, Equation (25) can be rewritten as

$$\dot{f}_{Ii}^{\text{mat}} = \int_{\mathsf{X}} \frac{\mathrm{L}N_I}{\mathrm{L}x_k} C_{kijl}^{\mathsf{r}\,T} \frac{\mathrm{L}\mathsf{m}_j}{\mathrm{L}x_l}\, \mathrm{d}\mathsf{X} \tag{28}$$

By implementation of the discretization technique to the velocity gradient term in Equation (28), the final applicable formulation for the material stiffness matrix can be derived as

$$\dot{f}_{Ii}^{\text{mat}} = \left[\int_{\mathsf{X}} \frac{\mathrm{L}N_I}{\mathrm{L}x_k} C_{kijl}^{\mathsf{r}\,T} \frac{\mathrm{L}N_J}{\mathrm{L}x_l}\, \mathrm{d}\mathsf{X} \right] \mathsf{m}_J \quad \text{or} \quad \dot{f}_{Ii}^{\text{mat}} = K_{IijJ}^{\text{mat}} \mathsf{m}_J \tag{29}$$

DOI: 10.1002/nme

Now, considering Equation (26), by implementation of discretization technique over the velocity gradient term and changing indices to comply with indices of Equation (29), the final formulation of geometric stiffness matrix can be written as

$$\dot{f}_{Ii}^{\text{geo}} = \int_{\Omega} \frac{\partial N_I}{\partial x_k} \tau_{kl} \frac{\partial N_J}{\partial x_l} \delta_{ij} \, d\Omega \; \dot{u}_J \quad \text{or} \quad \dot{f}_{Ii}^{\text{geo}} = K_{IijJ}^{\text{geo}} \dot{u}_J \tag{30}$$

The integrals of Equations (29) and (30) must be calculated numerically. Among varieties of different approaches, two methods are more prevalent; the Newton–Cotes and Gauss methods [32]. Despite the lower precision of the Newton–Cotes method, it provides the opportunity to choose the position of quadratures, which can be helpful wherever their configuration is a primary concern in numerical solution. As a practical guideline in the solution of Equation (21), the total external force is divided into several increments, in which each incremental load is implemented at the beginning of each step. At each step, the incremental displacement is derived numerically by solving the linearized equation (22). In this equation, the stiffness matrix K is the sum of material and geometric stiffnesses, i.e. Equations (29) and (30). It is obvious that the residual force is not satisfied by a linear solution, and as a consequence, the solution of Equation (22) must be continued in an iterative fashion as long as the norm of residual force becomes smaller than a prescribed value. In order to implement the equivalent continuum presented in the previous section, we need to make two main changes in a conventional nonlinear finite element. First, in the calculation of material stiffness matrix, the Truesdell stiffness matrix must be calculated via Equations (11) and (13). Second, in the implementation of Equation (30) the Cauchy stress must be calculated from Equations (6) and (8).

5. BOUNDARY CAUCHY–BORN MODEL

In the preceding section, the updated Lagrangian formulation is presented by the evaluation of Cauchy stress and Truesdell elasticity tensors at each integration point. Consider a fully atomistic model and its equivalent continuous model implemented in the nonlinear finite element method. It is clearly obvious that the position of quadratures in the continuous model may not coincide with atomic positions in the atomistic model. When the quadrature is located within the bulk of structure, i.e. it is not in the proximity of the surface, it is surrounded by identical atoms which experience the same atomic neighbors, and have similar material properties. As the quadratures should essentially reflect the behavior of surrounding material, it is quite rational to deduce that the properties of the quadrature can be assumed equal to a representative atom in the bulk of material. In fact, the representative atom is an atom that has all the possible neighbors within the cut-off radius of simulation. This assumption is implicitly expressed in all multi-scale methods based on the CB hypothesis [13, 17]. If the quadrature approaches to the adjacency of the structure's surface, the above assumption becomes invalid. It is primarily because the quadrature is immersed in a medium in which different atoms have varied neighboring list of atoms and thus, they have different characteristics. Therefore, the above definition of the representative atom for the integration points near the surface is somehow useless. In order to design a model which can appropriately describe the surface effect in nano-structures, one should in advance deal with the inhomogeneous nature of atomic medium near the surface.

In the Boundary Cauchy–Born model (BCB) developed here, it is emphasized that the quadrature must exhibit the governing circumstances on the lattice structure. The intrinsic notion of this novel

DOI: 10.1002/nme

method is principally embedded in an interpolation technique. In fact, if a quadrature is located in the surface, its properties can be then evaluated by means of interpolating information, i.e. the Cauchy stress and Truesdell elasticity tensors, from possible atomic positions next to this quadrature. In order to efficiently implement the technique, the concept of boundary CB elements is defined. Basically, three types of boundary CB elements are defined; including: the surface element, the edge element, and the corner element. In order to provide an applicable approach suitable for the simulation of structures with complicated shapes and geometries, the concept of boundary CB element is blended with the reference boundary CB element. In other words, in order to avoid the repetitious definition of a single conceptual object and use this object anywhere necessary, the reference boundary CB elements are defined in which all information are calculated and then mapped to real elements that may have arbitrary spatial configuration in the model.

Consider a line perpendicular to the surface of structure, by moving on this line toward the surface, the material undergoes a severe variances in material properties. It therefore indicates a potential zone, which can lead to high gradients in the model. Hence, the reference boundary CB elements are defined such that they have more quadratures in the direction perpendicular to the surface. In order to model the effect of surface in crystalline structures, the crucial step is to specify the cut-off radius of atomistic simulation. In modeling of the surface effect in metallic nano-structures, the 7th shell of atomic neighbors is considered here. It means that 134 atoms are assumed in the calculation of representative atom in the bulk of structure. This cut-off radius means that those atoms exposed to the effect of surface are up to the third atomic layer and, those of the fourth layer can be considered as the bulk atoms. Until now, the essential prerequisites are illustrated. In what follows, the reference boundary CB elements are defined.

5.1. Reference surface element

In the reference surface element, merely one of its sides is located on the surface of structure, as shown in Figure 2. In this element, the surface of element is perpendicular to the global z-direction and the center of element has a lower z component rather than surface nodes. According to Figure 2, each atom located in layers L_1 is identical to the representative bulk atom since it has 134 neighboring atoms. However, those atoms located in layers L_2, L_3 and L_4 have different neighbors with less than 134 atoms. It must be noted that the density of neighbors around each atom is absolutely different in z-direction. In other words, each atom of layer L_2 does not include

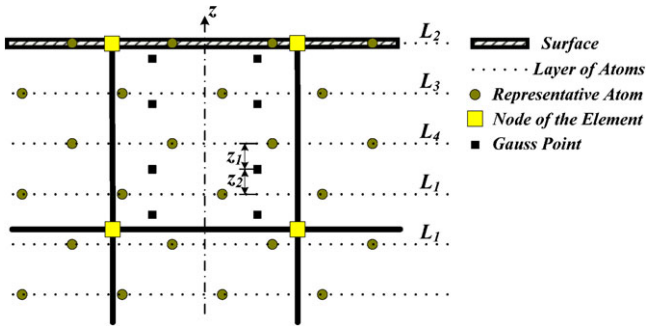

Figure 2. Description of reference surface element and its configuration with respect to the atomistic model.

DOI: 10.1002/nme

its upper neighboring atoms, while the atom in layer L_3 has acquired part of its upper neighbors. As only one side of element is located on the surface, all atoms of each layer have identical neighbor lists and consequently, identical properties.

In the boundary CB model, instead of defining a representative atom in the reference boundary elements, the representative atomic layer is defined. For instance, the representative atom of layer L_4 is called L_4, and in the outset of simulation, its characteristics are specified. For the calculation of information at any quadrature in the reference surface element, its position must be identified with respect to atomic layers. In other words, the atomic layers that the quadrature can inherit from them must be specified before the initiation of the simulation. In the BCB model, the integration point merely inherits information from the upper and lower layers. Considering the quadrature between the layer L_1 and L_4, as shown in Figure 2, if the required information at this quadrature is called I, this property should be calculated by interpolating the information from the upper L_4 and lower L_1 layers as

$$\mathsf{I}_Q = \frac{z_2}{z_1+z_2}\mathsf{I}_{L_4} + \frac{z_1}{z_1+z_2}\mathsf{I}_{L_1} \tag{31}$$

where $\mathsf{I}_Q, \mathsf{I}_{L_1}$ and I_{L_4} denote the desired characteristic at the quadrature, representative atom in the layers L_1 and L_4, respectively. As shown in Figure 2, z_1 and z_2 represent the distance from layers L_4 and L_1, respectively. Equation (31) presents a linear interpolation of data between two adjacent atomic layers. It is necessary to clarify that in the real atomistic model, there may not exist an atom right on the nearby layers of the integration point. In fact, in FCC lattice, two representative atoms together with the integration point do not coincide within one perpendicular line to the surface of structure. Hence, these three points may take numerous configurations in the space depending on their position. Closely investigating the set of all possible configurations, one may find a simplified assumption that these three points are located in a perpendicular line to the surface, as a quite rational average. The information at other integration points can be derived by the similar procedure presented in Equation (31).

In the BCB model, there is basically no constraint in the size of reference boundary element in the surface direction. Nevertheless, by enlarging the size of element in the z-direction, more layers are included that have no influence on the surface effect. As a consequence, more integration points are required to capture the surface effect which leads to dramatically increasing the computational cost. In addition, by increasing the number of integration points with the bulk properties of reference surface element, and due to limited number of nodal points, the effect of integration points to capture the surface properties mitigates. Therefore, we consider only four atomic layers within the reference surface element and so, the size of element in the surface direction is less than twice the lattice parameter.

5.2. Reference edge element

In the reference edge element, two surfaces of element are located on the surface of structure, as shown in Figure 3. In this case, the surfaces of element are perpendicular to the global x- and z-directions while the center of element should have less z and x components with respect to nodal points of intersection of two surfaces. In the edge element, the concept of atomic layers cannot be used and, each atom has its own neighboring list. As a result, it has a unique property which distinguishes it from other atoms. Considering the crystalline FCC structure, it can be observed that the integration points may be close to any of two configurations presented in Figure 3.

DOI: 10.1002/nme

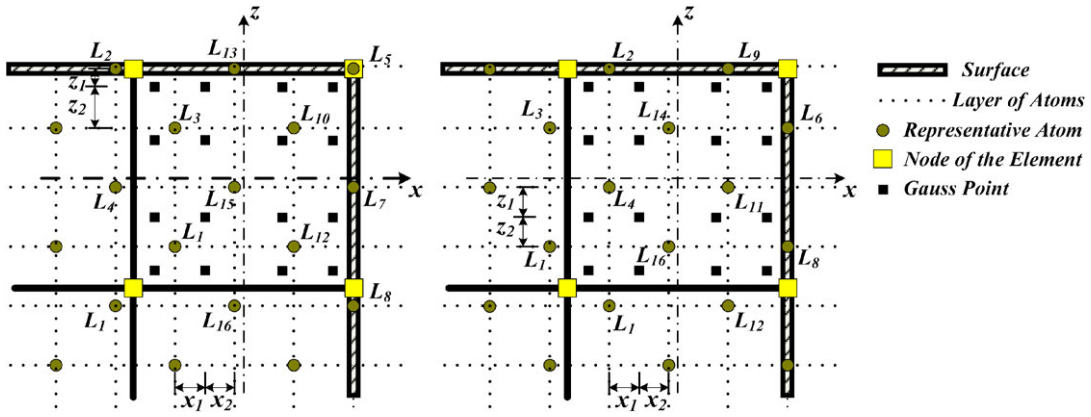

Figure 3. Description of reference edge elements and configuration of representative edge atoms with respect to integration points.

According to the pre-defined cut-off radius, there are 12 new representative edge atoms, in which their characteristics must be specified in the pre-processing phase.

Similar to the reference surface element, there are varieties of possible configurations for the positions of integration point and corresponding representative edge atoms. Meticulously, inquiring both configurations provided in Figure 3, there are probably four representative atoms within the proximity of each quadrature. As a rough estimation, it is considered that all four representative atoms along with the quadrature point are located in one surface which is perpendicular to the intersection of two surface sides. This rough assumption can be regarded as the average of possible configurations. It must be noted that we can increase the accuracy of computation by choosing the quadrature points close to representative atoms, if the Newton–Cotes method is used in the definition of quadrature points in the reference boundary elements. If the quadrature approaches to the representative edge atoms, its properties should become similar to the nearby representative edge atom. This observation explicitly alleges that for the purpose of interpolation in reference edge element, the conventional two-dimensional shape function of rectangular element can be employed. Thus, if the desired characteristic at the integration point is denoted by I_Q, this property can be derived as

$$I_Q = I_{L_i} N_{L_i}(x_Q, z_Q) + I_{L_j} N_{L_j}(x_Q, z_Q) + I_{L_k} N_{L_k}(x_Q, z_Q) + I_{L_l} N_{L_l}(x_Q, z_Q) \tag{32}$$

where $N_{L_i}(x_Q, z_Q)$ is the value of shape function of the L_i representative atom at the quadrature, and i, j, k and l denote the nearby representative atoms which are located on the vertices of a virtual square with side lengths equal to half the lattice parameter. It must be noted that since there are two surface sides in this type of element, the quadratures should be therefore increased in two directions. Furthermore, in order to better capture the edge effects, the dimensions of the element in two directions are set to include only four atomic layers in each direction.

5.3. Reference corner element

In the reference corner element, there are three sides of element need to represent the effect of surface. In the corner element, the three surface sides are pre-specified and the quadratures are

DOI: 10.1002/nme

increased in all directions. Similar to the reference surface and edge elements, the first step is to indicate the representative corner atoms. Owing to three-dimensional variations of properties in the corner element, the representative corner atoms cover each quadrature in three dimensions. Considering both continuous and discrete models simultaneously, it can be realized that there may be eight possible atomic positions near each quadrature, which can inherit its characteristics from them. These eight atoms are located on the vertices of a cube with sides equal to half the lattice parameter. It must be emphasized that in the atomistic model these eight atoms are used to represent the characteristics of quadrature. As the quadrature should have similar characteristics with its representative nearby atom, it can be deduced that its characteristics can be computed based on the interpolation shape functions of a cubic element. Therefore, the property of each quadrature can be evaluated as

$$\mathsf{I}_Q = \sum_{i=1}^{8} \mathsf{I}_{L_i} N_{L_i}(x_Q, y_Q, z_Q) \tag{33}$$

where $N_{L_i}(x_Q, y_Q, z_Q)$ is the value of shape function at the quadrature point.

6. NUMERICAL SIMULATION RESULTS

The implementation of BCB model developed here is one of the brilliant features of the multi-scale method. The first and the most important step is the definition of reference boundary CB elements in the nonlinear FE program. The definition of boundary CB elements includes the determination of quadratures, their direction, representative atoms, and their characteristics. In the next step, the finite element mesh is generated, the boundary CB elements are specified, and the types of surface elements are recognized. Finally, the rotation matrix is computed for each element to map the information obtained in reference elements to the standard elements of the domain under investigation. Two main variables, which are necessary for the standard configuration, are the Cauchy stress and Truesdell elasticity tensors which can be mapped by

$$\mathsf{r}_{ij} = Q_{mi} Q_{nj} \mathsf{r}^*_{mn} \tag{34}$$

$$C_{ijkl} = Q_{mi} Q_{nj} Q_{kp} Q_{lq} C^*_{mnpq} \tag{35}$$

where Q denotes the rotation tensor, and the asterisk indicates the calculated values in the reference element.

In order to evaluate the capability of BCB, the results of two finite element simulations are directly compared with fully atomistic models. Both models are relaxed under surface stress and no external load or displacement is exerted on the boundaries. The molecular dynamics (MD) simulations are performed by the MASS software developed by authors [24, 25, 33]. The Sutton–Chen potential is used in both continuous and discrete models. In order to exclude the effect of temperature in atomistic models, the MD simulations are performed by canonical ensemble at zero temperature using the Brendsen thermostat. The velocity-Verlet algorithm is employed as the finite difference method for the derivation of trajectories. In fact, the damped molecular dynamics used in simulations is equivalent to the energy minimization methods such as molecular statics which locally minimizes the total potential energy of the system. In fact, it is implicitly expressed that

DOI: 10.1002/nme

the deformation predicted by the CB hypothesis minimizes the total potential energy of infinite lattice.

The finite element models are simulated using the linear and quadratic hexahedral elements. While $2 \times 2 \times 2$ Gaussian quadratures are used for the internal elements, the numerical integration of boundary CB elements is performed using 4 and 5 quadratures in the direction of surface. In order to investigate the effect of quadrature positions in boundary CB elements, both the Newton–Cotes and Gauss quadratures methods are applied in the numerical simulations. The distributions of stresses are obtained for two different models and the results are compared. The nonlinear finite element models are solved by the full Newton–Raphson technique.

6.1. Modeling of nano-scale cube

The first example is chosen to demonstrate the capability of BCB model in surface modeling of a nano-scale cube. An infinite FCC crystal is simulated and the results are compared with fully atomistic model. A cubic gold specimen, with each side of 8.16 Å, is relaxed under direct effect of surface in both discrete and continuous models. The MD sample is consisted of 32 000 atoms. The evolution of stress components is performed at the center, surface and edge lines of the cube, as shown in Figure 4. In Figure 5, the contours of stress component r_x are shown for the molecular dynamics and BCB models. As can be seen, the BCB model can effectively capture the surface effect over the surface of cube, particularly the highest values of stress can be observed along the edge parallel to the x-direction. The stress concentration at the edges of BCB model is in complete agreement with that obtained by the MD model. In Figure 6, the contours of stress component r_x are shown at a section of cube for the BCB and MD models. Clearly, it shows that the stress is positive at the edges and boundaries of cube. By approaching to the center of cube, the stress reduces to a negligible negative value. The physical interpretation of this observation reveals that the outer surface of cube is stretched by the inner part to increase the electron density at the boundary atoms. In contrast, the inner core is compressed by the outer surface according to the third Newtonian Law.

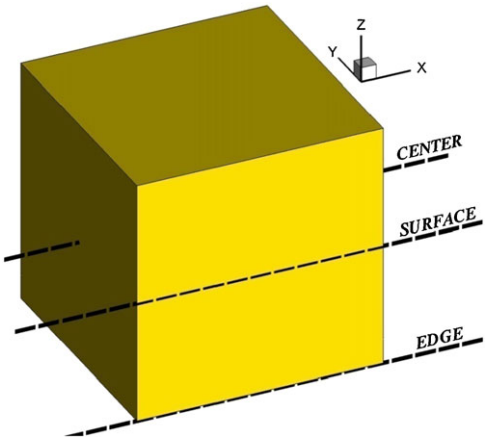

Figure 4. Modeling of nano-scale cube: the evolution of stress components at the center, surface and edge lines of the cube.

DOI: 10.1002/nme

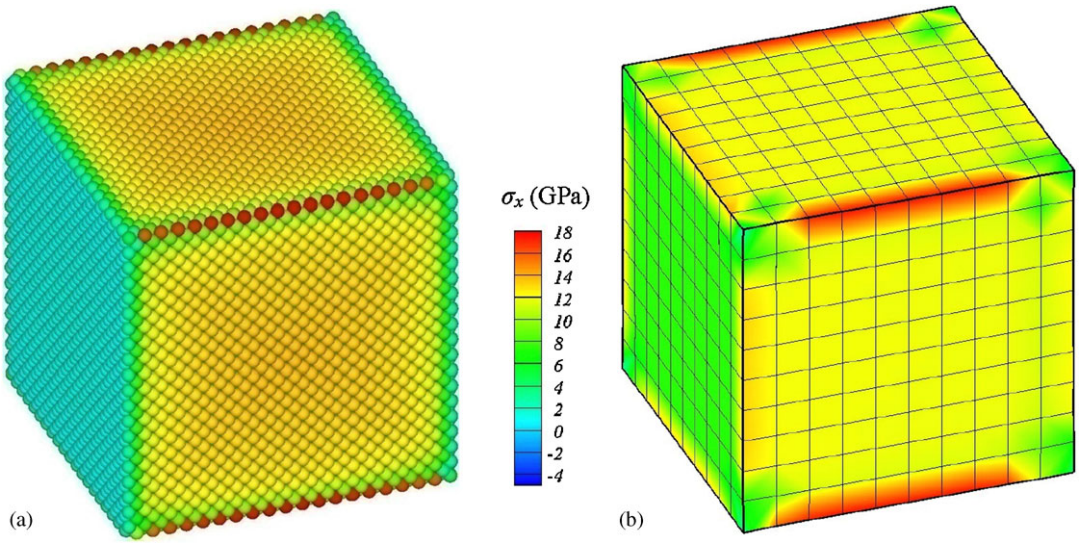

Figure 5. The contours of stress component σ_x: (a) MD model and (b) BCB model.

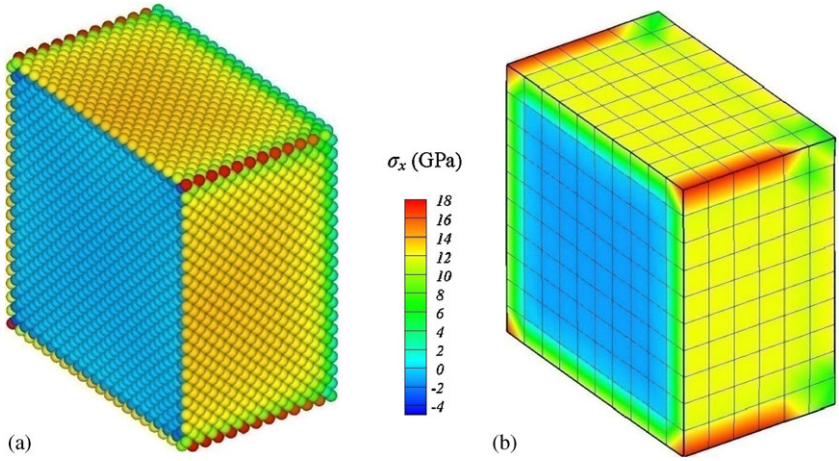

Figure 6. The evolution of σ_x stress contours in the core and surface of the cubic structure: (a) MD model and (b) BCB model.

In Figures 7 and 8, the evolution of stresses σ_x and σ_y is shown along the line passed through the center of cube for the BCB and MD models. In these figures, the results of BCB simulations with Gauss quadratures are denoted by 'G' and those of Newton–Cotes by 'NC'. Clearly, it can be seen from Figure 7 that the value of stress increases at the boundaries, and decreases at the inner part of the cube. Obviously, the boundary CB model with 20-noded quadratic elements is in good agreement with that obtained by the MD model. In Figure 8, the stress is

DOI: 10.1002/nme

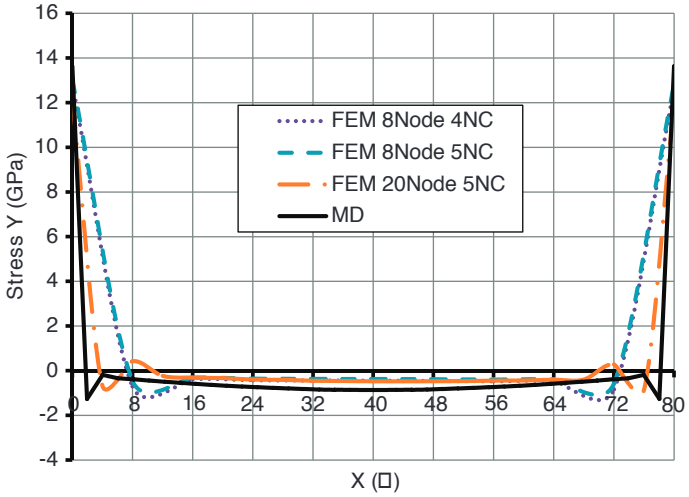

Figure 7. The evolution of stress σ_y along the line passed through the center of cube.

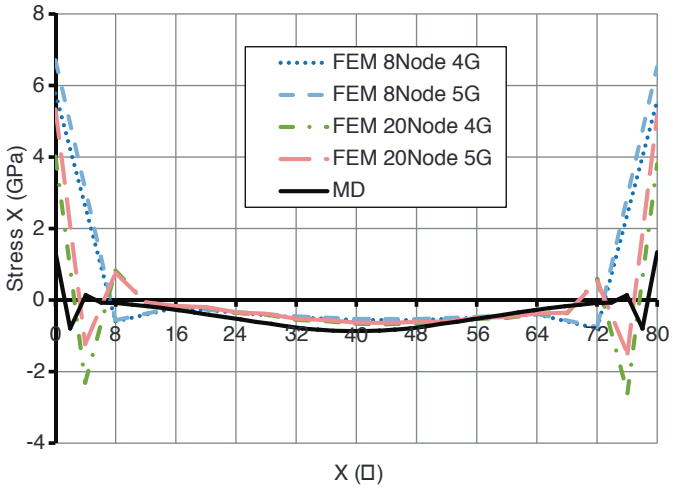

Figure 8. The evolution of stress σ_x along the line passed through the center of cube.

plotted along the line passed through the center of cube for the BCB and MD models. In both models, the stress has negative value in the inner part and becomes positive by moving to the boundaries. Obviously, the trend of stress over the surface is of strong interests with the BCB model.

In Figure 9, the evolution of stress σ_y is presented along the line passed through the surface of cube depicted in Figure 4. The MD simulation demonstrates that the value of stress is high at the center of surface, its value decreases by approaching to the edges of cube, and in a few angstroms

DOI: 10.1002/nme

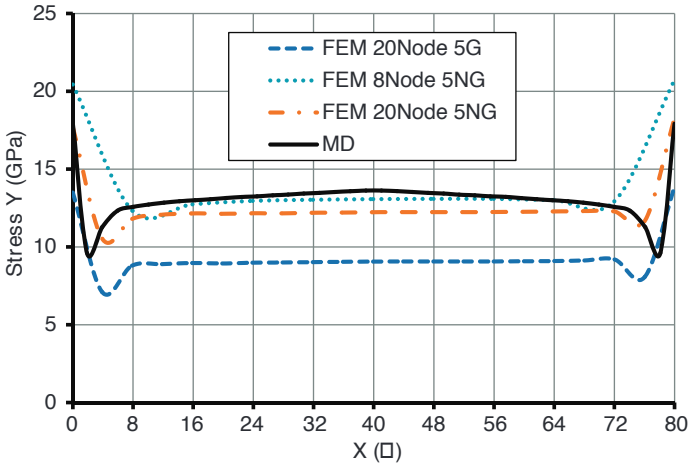

Figure 9. The evolution of stress σ_y along the line passed through the surface of cube.

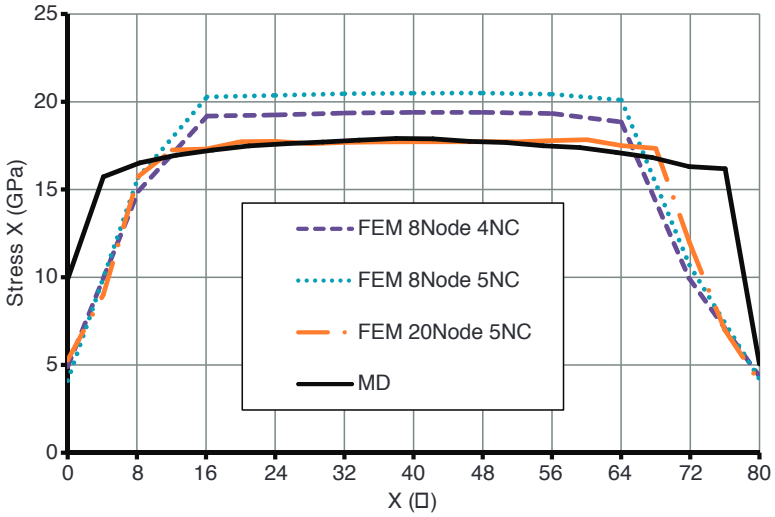

Figure 10. The evolution of stress σ_x along the line passed through the surface of cube.

it shows the stress concentration at the edges of cube. This trend can be also observed by all finite element models; however, the results significantly improve by the Newton–Cotes integrations algorithm. It shows that despite the lower precision of Newton–Cotes method, the results are more close to MD simulation since it provides the opportunity to choose the position of quadratures in the continuous model. In Figure 10, the evolution of stress σ_x is presented along the line passed through the surface of cube. It can be seen that for the distance from 16 to 64 Å, the BCB model with 20-noded quadratic elements and 5 Newton-Cotes integration points are almost identical to MD simulation.

DOI: 10.1002/nme

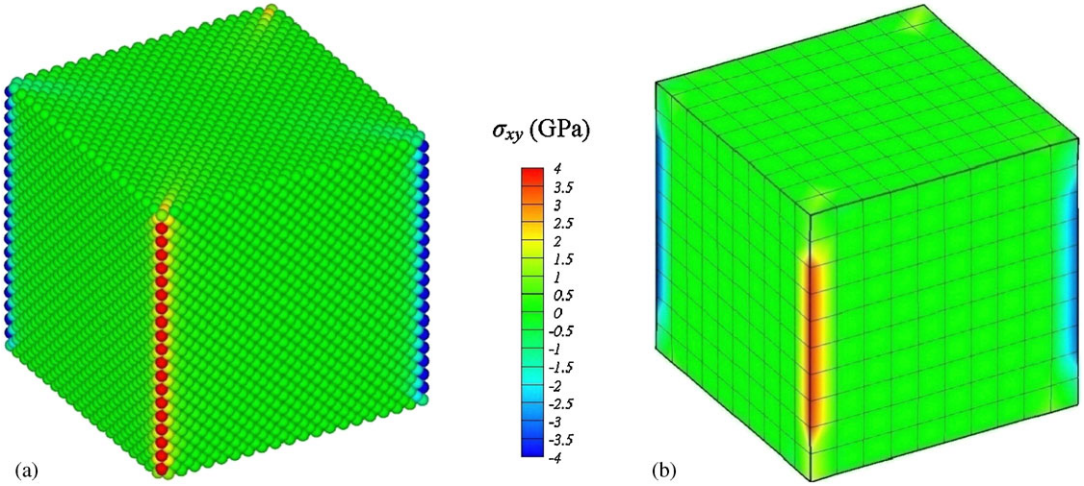

Figure 11. The contours of shear stress τ_{xy}: (a) MD model and (b) BCB model.

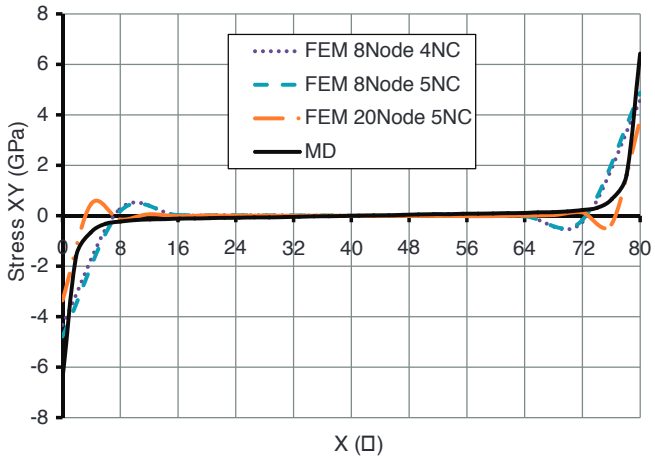

Figure 12. The evolution of shear stress τ_{xy} along the line passed through the surface of cube.

In Figure 11, the contours of shear stress τ_{xy} are shown for the MD and BCB models. This figure displays the most prominent features of the boundary CB technique in the modeling of surface effects, particularly at the edges of cubic specimen. In Figure 12, the evolution of shear stress τ_{xy} is plotted along the line passed through the surface of cube. A good agreement can be seen between the MD and BCB models. This example adequately presents the efficiency of boundary CB model in displaying the behavior of surface stress over the body of cubic structure. It is shown that it precisely captures the distribution of stresses at the edges and corners. Furthermore, the results indicate that the Newton–Cotes integration points improve the distribution of surface stress significantly.

DOI: 10.1002/nme

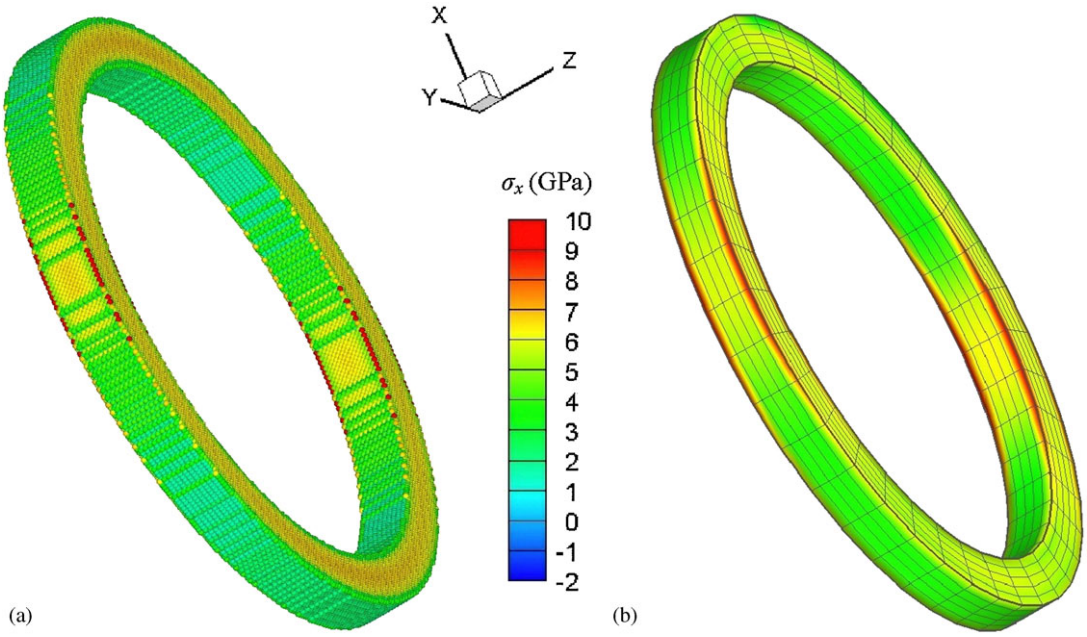

Figure 13. Modeling of nano-scale ring; The evolution of stress σ_x contours; (a) MD model and (b) BCB model.

6.2. *Modeling of nano-scale ring*

The second example is chosen to demonstrate the capability of boundary CB method in modeling the surface effect in curved structures. A nano-scale ring is simulated by the BCB technique, as shown in Figure 13, and the results are compared with a fully atomistic model. The internal and external radii are 205.5 and 244.4 Å, respectively, and the height of the ring is 38.9 Å. The Sutton–Chen inter-atomic potential is used in both models and the silver constants are employed in numerical analyses. The MD model consisted of 130 000 atoms, which are extracted from a rectangular lattice in [1 0 0], [0 1 0] and [0 0 1] crystalline directions. The finite element models are constructed using 1500 8-noded linear hexahedral elements and 1000 20-noded quadratic hexahedral elements.

In Figure 13, the contours of stress distribution σ are shown for the MD and BCB models. The stress distributions at the surface and edges of BCB model are in complete agreement with those obtained by the MD model. Obviously, the surfaces parallel to the z-plane are influenced by the surface effect. Furthermore, both models represent that the stress has maximum values in the circumferential plans parallel to the x-direction. In order to quantitatively compare the results of continuous and discrete models, the evolution of stress σ_y is plotted along the line parallel to the x-direction passed through the mid-height of the ring, as shown in Figure 14. As can be observed, the stress has its maximum values over the surfaces and minimum value in the center of cross section of the ring. It shows that the BCB model with 20-noded quadratic elements and 5 Newton-Cotes integration points are more reliable. In order to investigate on the authenticity of results derived at the edges of the ring, the evolution of stress σ_x is plotted

DOI: 10.1002/nme

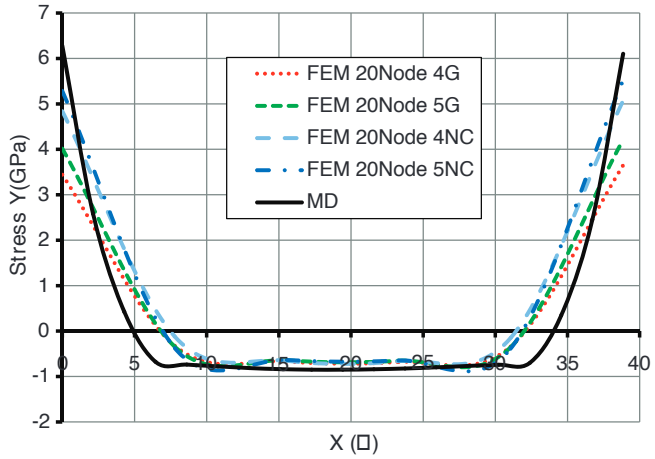

Figure 14. The evolution of stress σ_y along the line parallel to the x-direction passed through the mid-height of the ring.

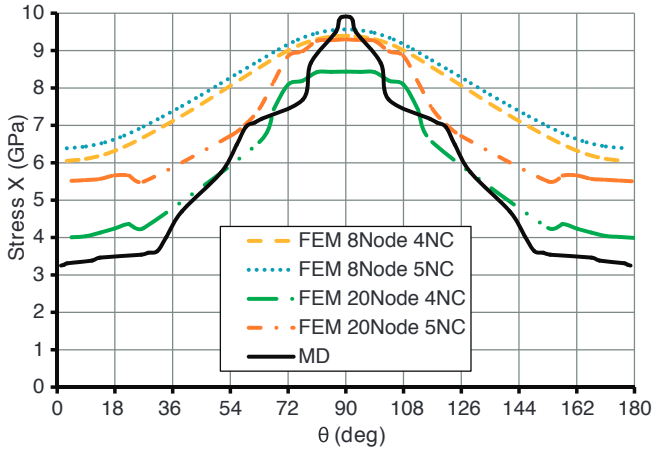

Figure 15. The evolution of stress σ_x along the half of the exterior circumference of ring.

along the half of exterior circumference of the ring, as shown in Figure 15. According to this figure, the linear FE model exhibits a highly-smoothed behavior; however, the quadratic FE model has captured the stair-like results derived from the MD simulation. In Figure 16, the contours of shear stress distribution are shown for the MD and BCB models. A good agreement can be seen between the MD and BCB models. Finally, the evolution of shear stress is plotted along the half of exterior circumference of the ring in Figure 17. Obviously, the BCB model provides a highly homogenized sinusoidal trend, particularly using the Newton–Cotes quadratures technique.

DOI: 10.1002/nme

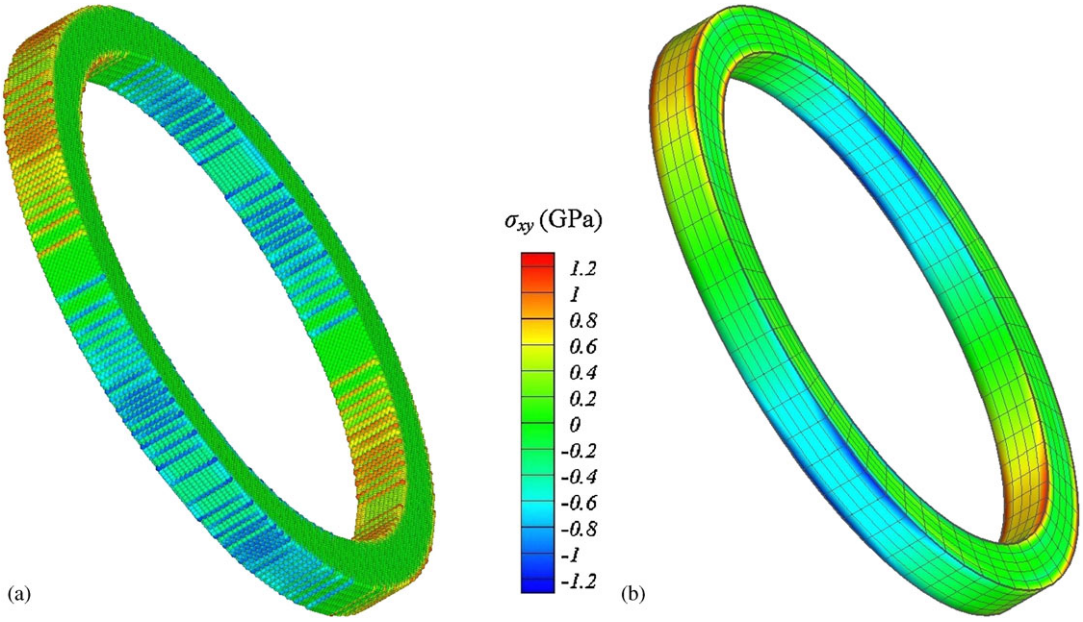

Figure 16. The evolution of shear stress σ_{xy} contours: (a) MD model and (b) BCB model.

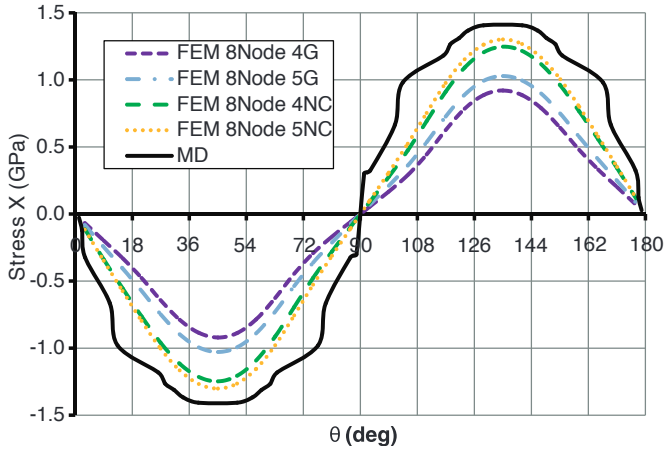

Figure 17. The evolution of shear stress σ_{xy} along the half of the exterior circumference of ring.

7. CONCLUSION

In the present paper, the BCB model was developed to investigate the surface effect in crystalline nano-structures since it plays an important role in its overall mechanical behavior. The technique was applied by the definition of reference boundary elements to capture the surface stress effect

DOI: 10.1002/nme

at the surface, edge and corner of structure. The surface effect was captured in the finite element method based on the intrinsic function of quadratures, called as an indicator of material behavior. The information of quadratures was derived by interpolating the data from probable representative atoms in their proximity. The nonlinear finite element method was applied to evaluate the capability of BCB model. The combination of element concept and surface modeling notion led to the production of the reference boundary element, which was classified into three distinct classes; the reference surface element, reference edge element, and reference corner element. By shrinking the size of structure, the total volume of the boundary CB elements becomes considerable with regard to overall volume of the structure. This leads to the predomination of boundary effect in model which indicates that this model can exhibit the inherent size-dependent characteristic of nano-structures.

Despite the elegant notions provided in analytical models [4, 12], they are generally restricted to simple geometries and boundary conditions. It is noteworthy to be expressed that these analytical approaches require additional atomistic simulations to obtain surface properties. As the technique proposed here is based on the well-known CB hypothesis, the necessity of extra atomistic simulation is relieved. In addition, this model can be implemented in the simulation of boundary-value problems along with any arbitrary form of boundaries. The BCB method developed here shows several aspects in comparison with the surface CB model recently proposed by Park *et al.* [13]. First, the BCB model is able to render the edge and corner effects which have profound effect in stress distribution over the body. Second, in the surface CB model, the finite element formulation is decomposed into two different parts and thus, the implementation of the method in a standard finite element code would be difficult. However, in the BCB technique presented here, the standard FE formulation is employed together with some modifications in the properties of quadratures. In fact, the simple notion behind this approach and its combination with element technology has provided a model which can be easily implemented in a standard nonlinear finite element code. Indeed, this model is designed to be well suited for the object-oriented programming. Finally, in order to illustrate the authenticity of results derived by the BCB model, two numerical examples are solved and their results are directly compared with the fully atomistic model. As a practical guideline, the model can be readily introduced to the existing concurrent multi-scale methods, such as the quasicontinuum, the bridging scale, and the bridging domain. It is therefore enough to use the boundary CB elements in the outer surface of these models. In a future work, the BCB model will be developed to investigate the nonlinear size-dependent behavior of metallic nano-wires in elastic large deformation problems.

ACKNOWLEDGEMENTS

The senior author is grateful for the research support of the Iran National Science Foundation (INSF).

REFERENCES

1. Sander D. Surface stress: implications and measurements. *Current Opinion in Solid State and Materials Science* 2003; 7:51–57.
2. Cammarata RC. Surface and interface stress effects in thin films. *Progress in Surface Science* 1994; 46:35–71.
3. Gibbs JW. *The Collected Works of J. Willard Gibbs*. Longman: New York, 1928.
4. Gurtin ME, Murdoch AI. Surface stress in solids. *International Journal of Solids and Structures* 1978; 14:431–440.
5. Gurtin ME, Murdoch AI. A continuum theory of elastic material surfaces. *Archives of Rational Mechanics and Analysis* 1975; 57:291–323.

DOI: 10.1002/nme

6. Miller RE, Shenoy VB. Size-dependent elastic properties of nanosized structural elements. *Nanotechnology* 2000; 11:139–147.
7. Shenoy VB. Atomistic calculations of elastic properties of metallic FCC crystal surfaces. *Physical Review B* 2005; 71:94–104.
8. Lim CW, He LH. Size-dependent nonlinear response of thin elastic films with nano-scale thickness. *International Journal of Mechanical Sciences* 2004; 46:1715–1726.
9. He LH, Lim CW, Wu BS. A continuum model for size-dependent deformation of elastic films of nano-scale thickness. *International Journal of Solids and Structures* 2004; 41:847–857.
10. Sharma P, Ganti S, Bhate N. Effect of surfaces on the size-dependent elastic state of nano-inhomogeneities. *Applied Physics Letters* 2003; 82:535–537.
11. Wei G, Shouwen Y, Ganyun H. Finite element characterization of the size-dependent mechanical behaviour in nanosystems. *Nanotechnology* 2006; 17:1118–1122.
12. Dingreville R, Qu J, Cherkaoui M. Surface free energy and its effect on the elastic behavior of nano-sized particles, wires and films. *Journal of the Mechanics and Physics of Solids* 2005; 53:1827–1854.
13. Park HS, Klein PA, Wagner GJ. A surface Cauchy–Born model for nanoscale materials. *International Journal for Numerical Methods in Engineering* 2006; 68:1072–1095.
14. Park HS, Klein PA. Surface Cauchy–Born analysis of surface stress effects on metallic nanowires. *Physical Review B* 2007; 75:085408.
15. Park HS, Klein PA. A surface Cauchy–Born model for silicon nanostructures. *Computer Methods in Applied Mechanics and Engineering* 2008; 197:3249–3260.
16. Tadmor EB, Ortiz M, Phillips R. Quasicontinuum analysis of defects in solids. *Philosophical Magazine A* 1996; 73:1529–1563.
17. Shenoy VB, Miller RE, Tadmor EB, Rodney D, Phillips R, Ortiz M. An adaptive finite element approach to atomic scale mechanics: the quasicontinuum method. *Journal of the Mechanics and Physics of Solids* 1999; 47:611–642.
18. Liu WK. Bridging scale methods for nanomechanics and materials. *Computational Methods in Applied Mechanics and Engineering* 2006; 195:1407–1421.
19. Xiao SP, Belytschko T. A bridging domain method for coupling continua with molecular dynamics. *Computational Methods in Applied Mechanics and Engineering* 2004; 193:1645–1669.
20. Tang Z, Zhao H, Li G, Aluru NR. Finite-temperature quasicontinuum method for multiscale analysis of silicon nanostructures. *Physical Review B* 2006; 74:064110.
21. Born M, Huang K. *Dynamic Theory of Crystal Lattices*. Oxford University Press: Oxford, 1954.
22. Malvern LE. *Introduction to the Mechanics of a Continuous Medium*. Prentice-Hall: Englewood Cliffs, NJ, 1968.
23. Ericksen JL. *The Cauchy and Born Hypotheses for Crystals*, *Phase Transformations and Material Instabilities in Solids*. Academic Press: New York, 1984; 61–77.
24. Khoei AR, Abdolhosseini Qomi MJ, Kazemi MT, Aghaei A. An investigation on the validity of Cauchy–Born hypothesis using Sutton–Chen many-body potential. *Computational Materials Science* 2009; 44:999–1006.
25. Aghaei A, Abdolhosseini Qomi MJ, Kazemi MT, Khoei AR. Stability and size-dependency of Cauchy–Born hypothesis in three-dimensional applications. *International Journal of Solids and Structures* 2009; 46:1925–1936.
26. Wu HC. *Continuum Mechanics and Plasticity*. Chapman & Hall: London, 2005.
27. Ackland GJ, Vitek V. Many-body potentials and atomic-scale relaxations in nobel-metal alloys. *Physical Review B* 1990; 41(9):10324.
28. Sutton AP, Chen J. Long-range Finnis–Sinclair potentials. *Philosophical Magazine A* 1990; 61:139–146.
29. Rafii-Tabar H. Modelling the nano-scale phenomena in condensed matter physics via computer-based numerical simulations. *Physics Reports* 2000; 325:239–310.
30. Khoei AR. *Computational Plasticity in Powder Forming Process*. Elsevier: Amsterdam, 2005.
31. Belytschko T, Liu WK, Moran B. *Nonlinear Finite Elements for Continua and Structures*. Wiley: Chichester, New York, 2000.
32. Zienkiewicz OC, Taylor RL. *The Finite Element Method*. Butterworth-Heinmann: Oxford, 2000.
33. MASS program. Available from: WWW.NANO-MASS.COM.

DOI: 10.1002/nme